mRNA-Based Designer APCs Elicit Robust CD8$^+$ and CD4$^+$ T Cell Responses

Toan Van Le[1], Shota Imai[1], Iriya Fujitsuka[1], Makie Ueda[1] Sayuri Nakamae[3], Shusaku Mizukami[3], Rikinari Hanayama[1,2†] and Tomoyoshi Yamano[1,2†]

1. Department of Immunology, Graduate School of Medical Sciences, Kanazawa University, Kanazawa, Japan
2. WPI Nano Life Science Institute (NanoLSI), Kanazawa University, Kanazawa, Japan
3. Department of Immune Regulation, SHIONOGI Global infectious Disease Division, Institute of Tropical Medicine, Nagasaki University, Nagasaki, Japan

[†]Correspondence to T.Y (tomoyoshi.yamano@med.kanazawa-u.ac.jp) or R.H (rikinari-hanayama@umin.ac.jp)

Running title: Designer cells for T cell differentiation

Abstract

mRNA-based therapeutics have demonstrated notable success in SARS-CoV-2 vaccines and are emerging in cancer immunotherapy. However, conventional mRNA cancer vaccines are limited by the low immunogenicity of tumor-associated and neoantigens. We addressed this limitation by formulating a modular, liposome-based mRNA cocktail comprising three distinct mRNAs encoding tumor antigen, the co-stimulatory molecule CD80, and membrane-tethered IL-2. Administration of this mRNA mixture transforms somatic cells into 'designer antigen-presenting cells (APCs)' in vivo, which simultaneously express the antigen, a co-stimulatory molecule, and a cytokine. These designer APCs more effectively activated tumor antigen-specific $CD8^+$ T cells than mRNA encoding the antigen alone and elicited robust anti-tumor immune responses. In addition, substituting IL-2 in the mRNA mixtures with membrane-tethered IL-12 led to the expansion and differentiation of endogenous antigen-specific Th1 helper T cells in vivo. Importantly, this platform activated NY-ESO-1-specific $CD8^+$ T cells both in human PBMCs in vitro and in HLA-A*02:01-transgenic mice, highlighting its translational potential. This modular mRNA strategy reprograms somatic cells in situ into designer APCs, providing a flexible and translatable platform for precision immunotherapy.

Introduction

mRNA-based therapeutics have dramatically accelerated the development of infectious disease vaccines. This accelerated timeline is evident in the significant progress achieved in less than a year for SARS-CoV-2, a process that typically takes several years[1,2]. This advancement, highlighted by the practicality and safety of mRNA vaccines, has increased interest in mRNA therapeutics globally. As a result, the development of vaccines for various infectious diseases and cancer is being pursued[3,4].

In cancer immunotherapy, mRNA encoding cancer neoantigens is currently being advanced in clinical trials[4,5]. Recent efforts have focused on vaccines that encode multiple sequences of neoantigens found in cancer cells[6,7]. However, in the context of cancer vaccines, the effectiveness of mRNA on its own remains limited, often necessitating the concurrent use of immune checkpoint inhibitors and other anti-cancer treatments[8]. This highlights the need for more efficient methods to activate $CD8^+$ T cells for enhanced anti-tumor responses.

The delivery of mRNA into cells triggers a cascade of events, starting with its translation into proteins, which are subsequently degraded by the proteasome. The resulting peptides are then complexed with major histocompatibility complex class I (MHC I) molecules and displayed on the cell surface for recognition by $CD8^+$ T cells[9]. However, T cell activation is not solely dependent on T cell receptor (TCR) engagement; it also requires co-stimulatory signals[10]. While professional antigen-presenting cells (APCs) express these co-stimulatory molecules, non-APCs lack them and are unable to directly activate naïve $CD8^+$ T cells upon mRNA uptake. In such cases, cross-presentation by professional APCs becomes

72 essential[11]. Non-APCs that have taken up mRNA-encoded antigens rely on
73 antigen transfer to dendritic cells, particularly XCR1^{+} conventional type 1 DCs
74 (cDC1s), which are specialized for cross-presentation and subsequent activation
75 of CD8^{+} T cells[12]. This dependency implies that the therapeutic potential of mRNA
76 vaccines may be constrained by the efficiency of antigen handover and the
77 functionality of cross-presenting DC subsets. To address this limitation, recent
78 efforts have focused on the development of lipid nanoparticles (LNPs) that
79 preferentially target dendritic cells, including both cDC1s and migratory cDC2s.
80 By engineering ionizable lipids or formulating mRNA with DC-targeting delivery
81 platforms, such as lipid nanoparticles (LNPs) or lipoplexes (LPX), it is now
82 possible to selectively deliver mRNA into DCs. This targeted approach bypasses
83 the need for antigen transfer from non-APCs and enables direct expression of
84 antigen and co-stimulatory molecules within dendritic cells[13,14]. These delivery
85 systems have demonstrated enhanced CD8^{+} T cell priming and improved
86 therapeutic efficacy in preclinical cancer models, reinforcing the rationale for
87 APC-directed mRNA delivery as a key component of next-generation cancer
88 vaccines.
89 In this study, we propose a novel approach to further enhance mRNA vaccine
90 efficacy by introducing mRNA constructs that encode not only tumor antigens, but
91 also co-stimulatory molecules and cytokines, thereby transiently reprogramming
92 recipient cells into ‘designer APCs’. This strategy complements the conventional
93 reliance on natural APC subsets by functionally reprogramming transfected cells
94 to acquire key immunostimulatory features, thereby providing an alternative route
95 for antigen presentation. These designer APCs are capable of directly activating

96 $CD8^+$ T cells and orchestrating a strong cytotoxic immune response. Moreover,
97 substituting IL-2 with cytokines such as IL-12 enables the in vivo differentiation of
98 antigen-specific Th1 helper T cells, highlighting the potential of this strategy to
99 precisely modulate T cell differentiation in a context-dependent manner.
100

101 **Result**

102 **Generation of designer APCs for activation of antigen-specific $CD8^+$ T cells**

103 To engineer designer APCs capable of activating antigen-specific $CD8^+$ T cells,
104 we synthesized a set of mRNAs encoding OVA-MITD (a model antigen containing
105 OT-I and OT-II epitopes, fused to a minimal MHC class I trafficking domain (MITD
106 to enhance antigen presentation)[15], the costimulatory molecule CD80, and
107 membrane-anchored IL-2 (achieved by fusing IL-2 to the extracellular domain of
108 CD8α). Plasmids used for in vitro transcription were engineered to include a 128-
109 nucleotide poly(A) tail for enhanced stability and incorporated N1-
110 methylpseudouridine triphosphate ($m^1\Psi TP$) in place of UTP (Fig.1a,
111 Supplementary Fig.1a-c)[15,16]. These mRNAs were transfected into MC38 cells,
112 resulting in robust cell surface expression of MHC I, CD80, and IL-2, as confirmed
113 by flow cytometry (Fig.1b, c). This indicated successful reprogramming of MC38
114 cells into 'designer APCs' simultaneously presenting antigen, co-stimulatory
115 molecule, and cytokine. When co-cultured with OVA-specific $CD8^+$ T cells (OT-I),
116 MC38 cells expressing all three components, OVA-MITD, CD80, and IL-2,
117 induced the most robust OT-I proliferation, compared to cells expressing OVA-
118 MITD alone or in combination with either CD80 or IL-2 (Fig.1d, e, Supplementary
119 Fig.1d, e).

120

121 **In vivo generation of designer APCs stimulates antigen-specific CD8$^+$ T**
122 **cells**

123 We examined whether in vivo generation of designer APCs could promote clonal
124 expansion of endogenous antigen-specific CD8$^+$ T cells. Mice were administered
125 control mRNA, OVA-MITD mRNA alone, or a mixture of OVA-MITD, CD80, and
126 IL-2 mRNAs once weekly for three consecutive weeks. All mRNAs were
127 formulated using the in vivo-jetRNA$^+$ liposomal delivery reagent for efficient
128 systemic delivery. One week after the final injection, spleens were harvested and
129 analyzed for OVA-specific CD8$^+$ T cells using MHC class I tetramer (Fig.2a).
130 Consistent with the in vitro results, OVA-tetramer$^+$ CD8$^+$ T cells expanded more
131 robustly in the combination group (56%) than in the OVA-MITD group (24.3%)
132 (Fig. 2b, c, Supplementary Fig. 2a). The expanded CD8$^+$ T cells exhibited a
133 CD44^{hi}CD62L^{low} phenotype, characteristic of effector or effector memory T cells,
134 and expressed IFN-γ (Fig.2d, Supplementary Fig.2b, c). Total splenocyte
135 numbers were comparable across all groups (Supplementary Fig.2d), suggesting
136 that the observed expansion of OVA-specific CD8$^+$ T cells was not due to non-
137 specific activation, but rather reflects a targeted immune response.

138 To assess therapeutic efficacy, we employed a tumor model in which E.G7 cells
139 (OVA-expressing EL-4 derivatives) were subcutaneously implanted into C57BL/6
140 mice. When tumors reached 100 mm^3, mice received weekly intravenous
141 injections of control mRNA, OVA-MITD mRNA alone or the combination mixture
142 for three weeks (Fig.2e). While OVA-MITD mRNA monotherapy delayed tumor
143 growth and extended survival relative to control, the combination treatment led to

144 even greater tumor suppression and prolonged survival (Fig.2f, g).

145 To elucidate the underlying mechanisms, we analyzed tumor-infiltrating
146 lymphocytes one week after mRNA administration (Fig.2h). $CD8^+$ T cells
147 constituted 4.6% of TILs in the OVA-MITD group, but increased to 13.5% in the
148 combination group (Fig.2i, j, Supplementary Fig.2e-g). Consistently, tumor
149 weights were significantly lower in the combination group (Supplementary Fig.2h).
150 Furthermore, a higher proportion of $CD8^+$ T cells expressed IFN-γ in the
151 combination group (Fig.2k), indicating enhanced infiltration and activation of
152 $CD8^+$ T cells in the tumor microenvironment. These results demonstrate that in
153 vivo-generated designer APCs expand antigen-specific $CD8^+$ T cells and elicit
154 potent anti-tumor immunity in the OVA antigen model.

155

156 **In vivo generation of designer APCs expands neoantigen-specific $CD8^+$ T**
157 **cells**

158 Using Rpl18 as a model neoantigen in the MC38 tumor system, we investigated
159 whether in vivo generation of designer APCs could expand neoantigen-specific
160 $CD8^+$ T cells. Mice were administered control mRNA, Rpl18-MITD mRNA alone,
161 or a mixture of Rpl18-MITD, CD80, and IL-2 mRNAs once weekly for three
162 consecutive weeks, in accordance with the administration protocol established in
163 the OVA model (Fig.3a, Supplementary Fig.3a). One week after the final injection,
164 spleens were harvested and analyzed for Rpl18-specific $CD8^+$ T cells using MHC
165 class I tetramers. Mice receiving Rpl18-MITD alone exhibited modest expansion
166 of tetramer-positive $CD8^+$ T cells, whereas the combination treatment induced
167 robust expansion and differentiation into $CD44^{hi}CD62L^{low}$ effector and effector

168 memory phenotypes (Fig.3b-d, Supplementary Fig.3b-d). As observed in the OVA
169 model, total splenocyte numbers remained unchanged across groups
170 (Supplementary Fig.3e), suggesting that the response was antigen-specific
171 rather than due to non-specific activation.
172 To assess therapeutic efficacy, Rpl18-MC38 tumors were subcutaneously
173 implanted and allowed to grow to approximately 100 mm^3. Following the same
174 weekly schedule as the OVA model, mice received either control mRNA, Rpl18-
175 MITD alone or the combination mRNA mixture once per week for three weeks
176 (Fig.3e). While Rpl18-MITD alone modestly delayed tumor growth, the
177 combination treatment resulted in significantly greater tumor suppression and
178 extended survival (Fig.3f, g). These results demonstrate that in vivo generation
179 of designer APCs not only promotes the expansion and functional differentiation
180 of neoantigen-specific $CD8^+$ T cells, but also enhances anti-tumor immunity and
181 improves survival compared to antigen-only mRNA vaccination.
182
183 **In vivo and in vitro evaluation of HLA-A*02:01-restricted responses induced**
184 **by humanized designer APCs**
185 To assess the function of designer APCs in an HLA-A*02:01-restricted humanized
186 mouse model, we used HHD mice, which express a chimeric MHC class I
187 molecule composed of the α1 and α2 domains of human HLA-A*02:01, the α3
188 domain of murine H-2Db, and human β2-microglobulin[18]. This model enables the
189 evaluation of HLA-A*02:01-restricted $CD8^+$ T cell responses in vivo. As a
190 representative tumor antigen, we selected NY-ESO-1, a cancer/testis antigen
191 widely expressed in various malignancies, and used its well-characterized HLA-

192 A*02:01-restricted epitope (amino acids 157-165)[19]. Mice were administered
193 either mRNA encoding NY-ESO-1-MITD alone or a combination of mRNAs
194 encoding NY-ESO-1-MITD, CD80, and IL-2 (Fig.4a, Supplementary Fig.4a). NY-
195 ESO-1-MITD alone failed to induce significant expansion of antigen-specific
196 $CD8^+$ T cells, whereas the combination treatment resulted in robust expansion
197 and differentiation of $CD44^{hi}CD62L^{low}$ effector/memory $CD8^+$ T cells (Fig.4b-d,
198 Supplementary.4b-d). Consistent with earlier results, total splenocyte numbers
199 remained unchanged across groups, indicating antigen-specific activation
200 (Supplementary Fig.4e). To assess cytotoxic activity, we performed an in vivo
201 killing assay using a 1:1 mixture of splenocytes pulsed with NY-ESO-1 peptide
202 (CellTrace Violet-labeled) and control peptide (CFSE-labeled), injected into
203 mRNA-treated mice seven days after the final injection (Fig.4e). NY-ESO-1
204 peptide-pulsed target cells were selectively eliminated in mice treated with the
205 mRNA mixture, but not in those receiving control mRNA or NY-ESO-1-MITD
206 mRNA alone (Fig.4f, g). These findings demonstrate that in vivo-generated
207 designer APCs can effectively induce functional antigen-specific CTLs within an
208 HLA-A*02:01-restricted setting.
209 Following in vivo evaluation in the HHD mouse model, we next examined the
210 function of designer APCs in a fully human context by performing in vitro co-
211 culture assays using TCR-transduced primary human PBMCs obtained from an
212 HLA-A*02:01-positive donor. A NY-ESO-1-specific TCR was introduced into
213 PBMCs derived from an HLA-A*02:01-positive healthy donor via lentiviral
214 transduction[17]. HEK293T cells were then transfected with either control mRNA,
215 NY-ESO-1-MITD mRNA alone, or a combination of NY-ESO-1-MITD, human

216 CD80, and membrane-anchored human IL-2 mRNAs to generate designer APCs
217 (Fig.4h, Supplementary Fig.4f, g). When co-cultured with the TCR-engineered T
218 cells, only the designer APCs expressing all three components induced robust T
219 cell activation, as demonstrated by the expansion of antigen-specific T cells and
220 the production of IFN-γ (Fig.4i, j, Supplementary Fig.4h, i).
221

222 **In vivo generation of designer APCs induces Th1 differentiation of antigen-**
223 **specific CD4$^+$ T cells**

224 To extend the functionality of designer APCs beyond CD8$^+$ T cell activation, we
225 engineered constructs to promote the differentiation of antigen-specific CD4$^+$
226 helper T cells. We designed mRNAs encoding membrane-anchored IL-12 and a
227 fusion protein comprising the OVA peptide fused to the MHC class II molecule
228 (MHC-II) I-A^b via a flexible linker, enabling direct epitope presentation without
229 intracellular processing (Fig.5a, Supplementary Fig.5a, b). Mice were
230 intravenously injected with either OVA-MHCII mRNA alone or a combination of
231 OVA-MHCII, CD80, and IL-12 mRNAs once weekly for two consecutive weeks.
232 One week after the final injection, spleens were harvested and analyzed by flow
233 cytometry using MHC-II tetramers to identify OVA-specific CD4$^+$ T cells (Fig.5b).
234 In mice treated with OVA-MHCII mRNA alone, only minimal expansion of antigen-
235 specific CD4$^+$ T cells was observed. In contrast, mice receiving the combination
236 mRNA mixture exhibited a marked increase in the frequency of MHC-II tetramer$^+$
237 CD4$^+$ T cells (Fig. 5c, d, Supplementary Fig.5c, d). Among these cells, 27%
238 expressed T-bet, a master regulator of Th1 differentiation[20] (Fig.5e, f,
239 Supplementary Fig.5e). Furthermore, upon ex vivo stimulation with OVA peptide,

240 a substantial proportion of $CD4^+$ T cells from the combination group produced
241 IFN-γ, confirming functional Th1 polarization (Fig.5g, Supplementary Fig.5f).
242 These results demonstrate that in vivo generation of designer APCs encoding an
243 MHC-II -linked antigen and IL-12 effectively promotes the expansion and Th1
244 differentiation of antigen-specific $CD4^+$ T cells.
245

246 **Discussion**

247 In this study, we demonstrated that co-delivery of mRNAs encoding antigens, co-
248 stimulatory molecules, and immunomodulatory cytokines can transiently
249 reprogram non-professional somatic cells into designer APCs in vivo, thereby
250 markedly enhancing neoantigen-specific $CD8^+$ T cell activation and expansion,
251 overcoming the low immunogenicity and neoantigen-prediction challenges of
252 conventional mRNA cancer vaccines. Furthermore, our results demonstrate that
253 the cytokine composition of the mRNA mixture can be tuned to direct $CD4^+$ T-cell
254 differentiation. For example, inclusion of IL-12 selectively promoted Th1
255 polarization of antigen-specific $CD4^+$ T cells. Several recent reports have
256 examined IL-12 mRNA as a stand-alone adjuvant. Aunins *et al.* showed that
257 formulating a separate IL-12 mRNA-LNP with an antigen-encoding mRNA-LNP
258 boosts $CD8^+$ T cell expansion and effector differentiation, but $CD4^+$ T cell help
259 remained modest[21]. Lapuente *et al.* achieved stronger Th1 skewing by anchoring
260 membrane-tethered IL-12 in an adjuvant mRNA construct, yet the effect was still
261 dependent on endogenous dendritic cells for optimal priming[22]. Unlike two-vial IL-
262 12 mRNA adjuvant protocols, the designer APC mRNA cocktail, comprising
263 antigen, CD80, and membrane-bound IL-12 effectively induced the in vivo

264 expansion and Th1 polarization of endogenous OVA-specific $CD4^+$ T cells, as
265 evidenced by T-bet expression and IFN-γ secretion. These findings highlight the
266 efficiency and modularity of the designer APC platform in directing antigen-
267 specific helper T cell responses.
268 Beyond IL-12, incorporating IL-15 or IL-21 could potentiate memory-precursor
269 $CD8^+$ T cells[24,25], whereas co-expression of co-stimulatory molecules such as 4-
270 1BBL or OX40L may further amplify effector functions[25,26]. These observations
271 underscore the platform's modularity: tailored combinations of antigens, co-
272 stimulatory molecules and cytokines can fine-tune T cell responses to specific
273 needs. Beyond cancer vaccines, the approach could be adapted to induce
274 antigen-specific tolerance in autoimmune or allergic disorders by co-encoding
275 inhibitory cytokines or other regulatory cues[28,29]. Other applications, such as the
276 induction of long-lived memory T cells or the avoidance of T cell exhaustion, may
277 also be explored by further customizing the mRNA payload. Thus, designer APCs
278 offer a flexible and precise platform for immune modulation in a variety of disease
279 contexts.
280 In this study, we employed commercially available liposomes for mRNA delivery,
281 which efficiently facilitated uptake and expression in recipient cells. However, the
282 use of more advanced delivery vehicles, such as LNPs or LPX engineered for
283 targeted delivery to dendritic cells, may further enhance transfection efficiency
284 and therapeutic outcomes. Recent reports have shown that dendritic-cell-
285 targeting LPX, such as those developed by BioNTech (e.g., BNT111) and others,
286 can improve antigen presentation and anti-tumor immunity[14,29,30]. Beyond lipid-
287 based carriers, viral-like particles, polymer-lipid hybrid nanoparticles, and

288 engineered extracellular vesicles represent additional platforms with the potential
289 to increase cargo stability, cellular specificity, and endosomal escape[31–33].
290 Integration of the designer APC mRNA platform with advanced delivery systems
291 may further enhance anti-tumor immunity by improving the precision and
292 efficiency of mRNA delivery to immune-relevant cell populations.
293 While these advantages are compelling, the potent immune activation achieved
294 with designer APCs raises safety considerations. Excessive or systemic
295 expression of pro-inflammatory cytokines could precipitate cytokine-release
296 syndrome or off-target tissue damage[34,35]. Rigorous dose-finding studies, and
297 tissue-restricted delivery will therefore be critical components of future
298 translational efforts.
299 In summary, our study establishes a novel and modular mRNA-based platform
300 for the in vivo generation of designer APCs, enabling the precise activation and
301 programming of antigen-specific T cell responses. This work provides a
302 foundation for future investigations into optimized mRNA formulations, advanced
303 delivery systems, safety engineering, and translational applications in cancer
304 immunotherapy and immune regulation.
305

306 **Methods**

307 **Cell lines**

308 The OVA-expressing murine lymphoma cell line, a derivative of EL4 (E.G7; ATCC,
309 CRL-2113) was cultured in RPMI 1640 (Nacalai Tesque) supplemented with 10%
310 fetal calf serum (FCS; Thermo Fisher Scientific), 1× non-essential amino acids
311 (Nacalai Tesque), 1 mM sodium pyruvate (Nacalai Tesque), 100 U/mL penicillin,

312 100 U/mL streptomycin (FUJIFILM Wako), and 0.05 μM 2-mercaptoethanol
313 (Thermo Fisher Scientific). To generate a stable MC38 cell line expressing mutant
314 Rpl18, we used a codon-optimized mouse Rpl18 gene containing the Q125R
315 mutation, which was previously reported in MC38 cells[36], but absent in the MC38
316 cells obtained from Kerafast. The mutated gene was fused to the transmembrane
317 domain of mouse CD8 via a 2A peptide and cloned into a third-generation
318 lentiviral vector (pLJM1, Addgene #91980) under the CMV promoter. MC38 cells
319 were transduced with lentiviral particles and stably expressed mutant Rpl18.
320 Rpl18-MC38 cells were cultured in DMEM (Nacalai Tesque) supplemented with
321 10% FCS, 2 mM L-glutamine (Nacalai Tesque), 1× non-essential amino acids,
322 1 mM sodium pyruvate, 10 mM HEPES (Nacalai Tesque), 50 μg/mL gentamicin
323 sulfate (Nacalai Tesque), and 100 U/mL penicillin-streptomycin. Human
324 embryonic kidney (HEK)-293T cells (ATCC, Cat# CRL-3216) were cultured in
325 DMEM supplemented with 10% FCS, 100 U/mL penicillin, and 100 U/mL
326 streptomycin. All cells were maintained at 37 °C in a humidified atmosphere
327 containing 5% CO_2.
328
329 **Mice**
330 C57BL/6 mice were purchased from Japan SLC. OT-I TCR transgenic mice[37] and
331 HLA-A*02:01 transgenic mice[18] mice were housed in a specific pathogen-free
332 facility. All animal experiments were performed following a protocol approved by
333 Kanazawa University.
334
335 **mRNA construct and in vitro transcription**

336 Plasmids for mRNA preparation were codon-optimized for murine expression
337 using VectorBuilder (VectorBuilder Ltd.). Each construct contained a consensus
338 Kozak sequence upstream of the start codon and three stop codons downstream
339 of the gene of interest. DNA fragments were synthesized by Eurofins Genomics
340 and cloned into the vector, which contains a T7 RNA polymerase promoter, 5′UTR,
341 coding region, 3′UTR, and a 128-base poly(A) tail. The 5′UTR, coding region, and
342 3′UTR sequences were based on those described in a previous study[38].
343 In vitro transcription was performed using the HiScribe® T7 High Yield RNA
344 Synthesis Kit (New England Biolabs). Transcribed mRNA was purified using the
345 Monarch® RNA Cleanup Kit (New England Biolabs). The quality of IVT-mRNA
346 was confirmed with the RNA ScreenTape kit (Agilent Technologies).
347
348 **mRNA transfection in vitro**
349 mRNA transfections were performed using the TransIT®-mRNA Transfection Kit
350 (Mirus Bio), a cationic lipid-based reagent. Briefly, mRNA was diluted in Opti-
351 MEM (Thermo Fisher Scientific) and mixed with TransIT-mRNA reagent
352 according to the manufacturer's protocol. The resulting RNA-lipid complexes
353 were added to the cells. Target protein expression was evaluated by flow
354 cytometry 18 hours after transfection.
355
356 **In vitro T cells proliferation assay**
357 Lymph node T cells were isolated from OT-I transgenic mice and labeled with
358 1 μM CellTrace™ Violet (CTV; Thermo Fisher Scientific) at 37 °C for 3 minutes. A
359 total of 2×10^5 CTV-labeled OT-I T cells were co-cultured with MC38 cells

360 transfected with mRNA encoding OVA-MITD, OVA-MITD + CD80, OVA-MITD +
361 membrane-anchored IL-2, or OVA-MITD + CD80 + membrane-anchored IL-2 at
362 a 4:1 T cell to MC38 cell ratio. Transfected MC38 cells were prepared according
363 to the mRNA transfection method described above. After 3 days of culture, T cell
364 proliferation was analyzed by flow cytometry.
365

366 **mRNA formulation and intravenous administration**

367 mRNA was formulated with in vivo-jetRNA+ (Polyplus) according to the
368 manufacturer's instructions. Briefly, mRNA was diluted in a suitable buffer and
369 mixed with in vivo-jetRNA+ reagent. A total of 200 μL of the resulting nanoparticle
370 suspension was intravenously injected into each mouse.
371

372 **In vivo tumor models and mRNA treatment regimen**

373 A total of 1×10^5 E.G7 tumor cells suspended in 200 μL PBS (FUJIFILM Wako)
374 were subcutaneously injected into the right flank of C57BL/6 mice. For the Rpl18-
375 MC38 tumor model, 5×10^5 Rpl18-MC38 cells suspended in a 1:1 mixture of
376 100 μL sterile PBS and 100 μL Matrigel (Corning) were injected into the same site.
377 For both tumor models, when tumors reached approximately 100 mm^3 in volume,
378 mice received weekly intravenous injections of mRNA for three consecutive
379 weeks. Treatment consisted of either OVA-MITD (5 μg) or Rpl18-MITD (5 μg)
380 combined with control mRNA (5 μg), or a mixture of OVA-MITD (5 μg) or Rpl18-
381 MITD (5 μg), CD80 mRNA (5 μg), and membrane-anchored IL-2 mRNA (5 μg). As
382 a negative control, control mRNA (15 μg) alone was administered. Akaluc-Venus
383 mRNA was used as the control mRNA in all treatment groups[39]. Tumor volumes

384 were measured two to three times per week using digital calipers and calculated
385 using the formula (length × width²) / 2, where length and width represent the
386 longest and shortest tumor diameters, respectively. Mice were euthanized when
387 tumors reached ≥2000 mm³, exhibited ulceration, or showed signs of severe
388 distress or moribundity, in accordance with predefined humane endpoint criteria.
389

390 **Isolation and Preparation of Tumor-Infiltrating Lymphocytes (TILs)**

391 Tumors were harvested and minced into ~2-3 mm fragments. Tissue dissociation
392 was performed using the Tumor Dissociation Kit, mouse (Miltenyi Biotec)
393 following the manufacturer's protocol. Briefly, tumor fragments were incubated
394 with enzyme mix in RPMI 1640 medium and processed on the GentleMACS™
395 Octo Dissociator (Miltenyi Biotec). The resulting single-cell suspension was
396 filtered through a 70 μm strainer to remove debris. Cells were washed twice with
397 PBS containing 2% FCS and subsequently counted. Purified TILs were
398 resuspended in complete RPMI 1640 medium containing 10% FCS for
399 subsequent flow cytometric analysis.
400

401 **TCR transduction of primary human T cells and co-culture experiment**

402 Peripheral blood mononuclear cells (PBMCs) from HLA-A*02:01-positive healthy
403 donors were cultured in X-VIVO 15 medium (Lonza) containing 5ng/mL human
404 IL-2 (BioLegend) and stimulated using Dynabeads Human T-Activator CD3/CD28
405 (Thermo Fisher Scientific). After 48 hours, the beads were removed, and the
406 activated T cells were transduced with a lentiviral vector encoding a TCR specific
407 for the NY-ESO-1 peptide (amino acids 157-165, SLLMWITQC)[17]. The medium

408 was subsequently refreshed three days after transduction. NY-ESO-1 TCR-
409 engineered T cells were labeled with 1μM CTV at 37 °C for 3 minutes.
410 Subsequently, 2×10^5 CTV-labeled T cells were co-cultured with HEK293T cells
411 transfected with either control mRNA, NY-ESO-1-MITD mRNA alone, or NY-ESO-
412 1-MITD combined with hCD80 and membrane-anchored hIL-2 mRNAs, at a T cell
413 to HEK293T cell ratio of 4:1. CD69 expression was measured after 24 hours of
414 co-culture, while IFN-γ production and T cell proliferation were evaluated by flow
415 cytometry three days after co-culture initiation.
416
417 **In vivo killing assay**
418 HLA-A*02:01 transgenic (HHD) mice were intravenously injected with
419 in vivo-jetRNA® complexes containing either a designer APC cocktail of
420 NY-ESO-1-MITD (5 μg), murine CD80 (5 μg), and membrane-anchored murine
421 IL-2-CD8 (5 μg); NY-ESO-1-MITD alone (5 μg); or Akaluc-Venus (15 μg) as a
422 negative control. Seven days later, 4×10^6 syngeneic target splenocytes,
423 prepared as a 1:1 mixture of NY-ESO-1-pulsed cells labeled with CTV and Wilms
424 Tumor 1 peptide-pulsed cells labeled with CFSE (Thermo Fisher Scientific), were
425 transferred intravenously. For peptide loading, HLA-A02:01 splenocytes
426 (1×10^7 cells /ml) were incubated with 10 μmol peptide for 2 h at 37 °C and
427 washed twice by centrifugation to remove unbound peptide. Twenty hours after
428 target-cell transfer, spleens were harvested, converted to single-cell suspensions,
429 and analyzed by flow cytometry; antigen-specific cytotoxicity was quantified from
430 the preferential loss of CTV^+ NY-ESO-1-pulsed cells relative to $CFSE^+$ control
431 peptide-pulsed cells.

432

433 **Antibodies and Flow Cytometry**

434 Antibody staining was performed according to standard procedures. Monoclonal
435 antibodies for surface staining, including antibodies against mCD3 (clone: 17A2),
436 mCD4 (clone: GK1.5), mCD8α (clone: 53-6.7), mCD44 (clone: IM7), mCD45
437 (clone: 30-F11), mCD62L (clone: MEL-14), mCD80 (clone: 16-10A1), mTCR-Vα2
438 (clone: B20.1), mH-2K^b bound to SIINFEKL-PE (clone: 25-D1.16), mIL-2 (clone:
439 JES6-5H4), hCD4 (clone: RPA-T4), hCD8 (clone: SK1), hCD69 (clone: FN50)
440 were purchased from BioLegend. Intracellular staining was performed using
441 antibodies against mIFN-γ (clone: XMG1.2), hIFN-γ (clone: 4S.B3), mT-bet
442 (clone:4B.10) in combination with the True-Nuclear Transcription Factor Buffer
443 Set (BioLegend). OVA-specific CD8$^+$ T cells, Rpl18-specific CD8$^+$ T cells, NY-
444 ESO-1-specific CD8$^+$ T cells, and OVA-specific CD4$^+$ T cells were quantified
445 using the following tetramers obtained from the NIH Tetramer Core Facility: H-
446 2K^b/OVA (257-264), H-2K^b/Rpl18 (KILTFDRL), HLA-A*02:01-H2K^b/NY-ESO-1
447 (SLLMWITQC), and I-A^b/OVA (323-339), respectively. Staining was performed
448 according to the manufacturer's instructions. For intracellular staining, cells were
449 fixed and permeabilized using the True-Nuclear Transcription Factor Buffer Set
450 (BioLegend) according to the manufacturer’s instructions. Briefly, cells were
451 incubated with fixation buffer for 60 minutes at room temperature in the dark,
452 followed by two washes with permeabilization buffer. Cells were then stained with
453 antibodies diluted 1:50 in permeabilization buffer for 45 minutes at room
454 temperature in the dark. After washing, cells were resuspended in FACS buffer
455 and subjected to flow cytometric analysis. Data were acquired using FACSDiva

software (BD). A FACSMelody (BD) was used for cell sorting. Data analysis was performed using FlowJo v.10.4.1 software.

ACKNOWLEDGMENTS

This work was supported by World Premier International Research Center Initiative (WPI), MEXT, Japan. We thank T. Yoshida for the helpful discussion. We thank the NIH Tetramer Core Facility for providing H-2K^b/OVA (257-264), H-2K^b/Rpl18 (KILTFDRL), HLA-A*02:01-H2K^b/NY-ESO-1 (SLLMWITQC), and I-A^b/OVA (323-339) tetramers. This work was supported by World Premier International Research Center Initiative (WPI), MEXT, Japan, Doctoral Program for World-leading Innovative & Smart Education (WISE) Program for Nano-Precision Medicine (TVL, IS), Japan Science and Technology Agency (JST) Fusion Oriented Research for Disruptive Science and Technology (FOREST) grant no. JPMJFR2115 (TY), and Practical Research for Innovative Cancer Control from the Japan Agency for Medical Research and Development (AMED) grant no. 24ck0106967h0001 (TY). ChatGPT (GPT-4, OpenAI) was used to refine the language and enhance readability. The authors take full responsibility for the final content.

Data availability

Upon reasonable request, data can be obtained from the corresponding author.

Author Contributions

T.V.L.: Conceptualization, Investigation, Data curation, Formal analysis,

Visualization, Writing-original draft. S.I., I.F., M.U.: Investigation, Methodology, Validation, Visualization. S.N., S.M.: Resources, Methodology. R.H.: Conceptualization, Supervision, Funding acquisition, Writing-review & editing. T.Y.: Conceptualization, Methodology, Supervision, Funding acquisition, Writing -review & editing.

Competing interests

The authors have no competing interests to disclose.

Ethics approval statement

All animal experiments were conducted in compliance with the ARRIVE guidelines (https://arriveguidelines.org/) and approved by the Animal Experimentation Committee of Kanazawa University (Kanazawa, Ishikawa, Japan; approval number: AP-204131). Female C57BL/6 mice aged 6 to 8 weeks and weighing 18-22 g were used. A total of 120 animals were included. Mice were group-housed (up to five per cage) under specific pathogen-free conditions, with ad libitum access to standard rodent chow and water, and maintained in a controlled environment (temperature, humidity, and 12-hour light/dark cycle). Environmental enrichment (e.g., nesting materials and shelters) was provided to minimize stress. At the end of the experiments,

500 animals were euthanized using CO_2 inhalation with a gradual fill rate, in

501 accordance with AVMA guidelines. PBMCs were collected with written informed

502 consent from single healthy volunteers following the guidelines approved by the

503 Research Ethics Committee of Kanazawa University.

504

505

506 **References**

507 1. mRNA vaccines — a new era in vaccinology | Nature Reviews Drug Discovery.

508 https://www.nature.com/articles/nrd.2017.243.

509 2. Polack, F. P. *et al.* Safety and Efficacy of the BNT162b2 mRNA Covid-19

510 Vaccine. *New England Journal of Medicine* **383**, 2603–2615 (2020).

511 3. Pardi, N. & Krammer, F. mRNA vaccines for infectious diseases — advances,

512 challenges and opportunities. *Nat Rev Drug Discov* **23**, 838–861 (2024).

513 4. Yaremenko, A. V., Khan, M. M., Zhen, X., Tang, Y. & Tao, W. Clinical advances

514 of mRNA vaccines for cancer immunotherapy. *Med* **6**, 100562 (2025).

515 5. Sayour, E. J., Boczkowski, D., Mitchell, D. A. & Nair, S. K. Cancer mRNA

516 vaccines: clinical advances and future opportunities. *Nat Rev Clin Oncol* **21**,

517 489–500 (2024).

518 6. Cafri, G. *et al.* mRNA vaccine–induced neoantigen-specific T cell immunity in

519 patients with gastrointestinal cancer. *J Clin Invest* **130**, 5976–5988 (2020).

520 7. Rojas, L. A. *et al.* Personalized RNA neoantigen vaccines stimulate T cells in
521 pancreatic cancer. *Nature* **618**, 144–150 (2023).

522 8. Duan, L.-J., Wang, Q., Zhang, C., Yang, D.-X. & Zhang, X.-Y. Potentialities
523 and Challenges of mRNA Vaccine in Cancer Immunotherapy. *Front. Immunol.*
524 **13**, (2022).

525 9. Neefjes, J., Jongsma, M. L. M., Paul, P. & Bakke, O. Towards a systems
526 understanding of MHC class I and MHC class II antigen presentation. *Nat Rev*
527 *Immunol* **11**, 823–836 (2011).

528 10. Chen, L. & Flies, D. B. Molecular mechanisms of T cell co-stimulation and co-
529 inhibition. *Nat Rev Immunol* **13**, 227–242 (2013).

530 11. Shi, Y. *et al.* Antigen transfer from non-APCs to APCs impacts the efficacy and
531 safety of protein- and mRNA- based vaccines. *Nano Today* **41**, 101326 (2021).

532 12. Del Prete, A. *et al.* Dendritic cell subsets in cancer immunity and tumor
533 antigen sensing. *Cell Mol Immunol* **20**, 432–447 (2023).

534 13. Oyama, R. *et al.* An Ionizable Lipid Material with a Vitamin E Scaffold as an
535 mRNA Vaccine Platform for Efficient Cytotoxic T Cell Responses. *ACS Nano*
536 **17**, 18758–18774 (2023).

537 14. Kranz, L. M. *et al.* Systemic RNA delivery to dendritic cells exploits antiviral
538 defence for cancer immunotherapy. *Nature* **534**, 396–401 (2016).
539 15. Kreiter, S. *et al.* Increased Antigen Presentation Efficiency by Coupling
540 Antigens to MHC Class I Trafficking Signals1. *The Journal of Immunology* **180**,
541 309–318 (2008).
542 16. Gallie, D. R. The cap and poly(A) tail function synergistically to regulate
543 mRNA translational efficiency. *Genes Dev* **5**, 2108–2116 (1991).
544 17. Karikó, K. *et al.* Incorporation of pseudouridine into mRNA yields superior
545 nonimmunogenic vector with increased translational capacity and biological
546 stability. *Mol Ther* **16**, 1833–1840 (2008).
547 18. Pascolo, S. *et al.* HLA-A2.1–restricted Education and Cytolytic Activity of
548 CD8+ T Lymphocytes from β2 Microglobulin (β2m) HLA-A2.1 Monochain
549 Transgenic H-2Db β2m Double Knockout Mice. *Journal of Experimental*
550 *Medicine* **185**, 2043–2051 (1997).
551 19. Bethune, M. T. *et al.* Isolation and characterization of NY-ESO-1–specific T
552 cell receptors restricted on various MHC molecules. *Proceedings of the*
553 *National Academy of Sciences* **115**, E10702–E10711 (2018).
554 20. Robbins, P. F. *et al.* Single and dual amino acid substitutions in TCR CDRs

555 can enhance antigen-specific T cell functions. *J Immunol* **180**, 6116–6131
556 (2008).
557 21. Szabo, S. J. *et al.* A Novel Transcription Factor, T-bet, Directs Th1 Lineage
558 Commitment. *Cell* **100**, 655–669 (2000).
559 22. Aunins, E. A. *et al.* An Il12 mRNA-LNP adjuvant enhances mRNA vaccine–
560 induced CD8 T cell responses. *Science Immunology* **10**, eads1328 (2025).
561 23. Peng, K., Zhao, X., Li, H., Fu, Y.-X. & Liang, Y. Membrane-IL12 adjuvant
562 mRNA vaccine polarizes pre-effector T cells for optimized tumor control.
563 *Journal of Experimental Medicine* **222**, e20241454 (2025).
564 24. Guo, J. *et al.* IL-15 functionalized biomimetic hybrid mRNA vaccine for
565 enhanced NSCLC immunotherapy via synergistic activation of T cells and NK
566 cells. *Materials Today Bio* **32**, 101914 (2025).
567 25. Kvistad, D. *et al.* IL-21 enhances influenza vaccine responses in aged
568 macaques with suppressed SIV infection. *JCI Insight* **6**, e150888.
569 26. Singh, R., Kim, Y.-H., Lee, S.-J., Eom, H.-S. & Choi, B. K. 4-1BB
570 immunotherapy: advances and hurdles. *Exp Mol Med* **56**, 32–39 (2024).
571 27. Sato, A. *et al.* Generation and characterization of OX40-ligand fusion protein
572 that agonizes OX40 on T-Lymphocytes. *Front. Immunol.* **15**, (2025).

573 28. Liu, Y. *et al.* Generation of tolerogenic antigen-presenting cells in vivo via the
574 delivery of mRNA encoding PDL1 within lipid nanoparticles. *Nat. Biomed. Eng*
575 1–15 (2025) doi:10.1038/s41551-025-01373-0.
576 29. Gál, L. *et al.* Restoration of Motor Function through Delayed Intraspinal
577 Delivery of Human IL-10-Encoding Nucleoside-Modified mRNA after Spinal
578 Cord Injury. *Research* **6**, 0056 (2023).
579 30. Sasaki, K., Sato, Y., Okuda, K., Iwakawa, K. & Harashima, H. mRNA-Loaded
580 Lipid Nanoparticles Targeting Dendritic Cells for Cancer Immunotherapy.
581 *Pharmaceutics* **14**, 1572 (2022).
582 31. Mahalingam, G. *et al.* SMART-lipid nanoparticles enabled mRNA vaccine
583 elicits cross-reactive humoral responses against the omicron sub-variants.
584 *Molecular Therapy* **32**, 1284–1297 (2024).
585 32. Yu, B. *et al.* Engineered cell entry links receptor biology with single-cell
586 genomics. *Cell* **185**, 4904-4920.e22 (2022).
587 33. Maeki, M. *et al.* Development of Polymer–Lipid Hybrid Nanoparticles for
588 Large-Sized Plasmid DNA Transfection. *ACS Appl Mater Interfaces* **16**, 2110–
589 2119 (2023).
590 34. Kojima, R. *et al.* Designer exosomes produced by implanted cells

591 intracerebrally deliver therapeutic cargo for Parkinson's disease treatment.
592 *Nat Commun* **9**, 1305 (2018).
593 35. Bitounis, D., Jacquinet, E., Rogers, M. A. & Amiji, M. M. Strategies to reduce
594 the risks of mRNA drug and vaccine toxicity. *Nat Rev Drug Discov* **23**, 281–
595 300 (2024).
596 36. Wang, J. *et al.* Recent Advances in Lipid Nanoparticles and Their Safety
597 Concerns for mRNA Delivery. *Vaccines (Basel)* **12**, 1148 (2024).
598 37. Hos, B. J. *et al.* Identification of a neo-epitope dominating endogenous CD8
599 T cell responses to MC-38 colorectal cancer. *OncoImmunology* **9**, 1673125
600 (2020).
601 38. Hogquist, K. A. *et al.* T cell receptor antagonist peptides induce positive
602 selection. *Cell* **76**, 17–27 (1994).
603 39. Gan, L.-M. *et al.* Intradermal delivery of modified mRNA encoding VEGF-A in
604 patients with type 2 diabetes. *Nat Commun* **10**, 871 (2019).
605 40. Single-cell bioluminescence imaging of deep tissue in freely moving animals
606 | Science. https://www.science.org/doi/10.1126/science.aaq1067.
607
608 **Fig 1. Generation of designer APCs for activation of antigen-specific CD8$^+$**
609 **T cells**

610 (a) Schematic of each mRNA construct encoding OVA-MITD, mouse CD80 or
611 membrane-anchored mouse IL-2. 5′ cap, 5′ UTR, open reading frame, 3′ UTR
612 and 128-nt poly(A) tail are indicated. (b) Co-culture scheme. MC38 cells were
613 harvested 18 h after mRNA transfection, mitomycin C (MMC)-treated, and co-
614 cultured with CellTrace Violet-labelled OT-I $CD8^+$ T cells. (c) Flow-cytometric
615 analysis of surface OVA-K^b complexes, CD80, and membrane-anchored IL-2 on
616 MC38 cells 18 h after transfection. Filled gray histograms: mock-transfected
617 MC38 cells; open black histograms: mRNA-transfected cells. Proliferation was
618 analyzed 72 h later. (d) Frequencies of OT-I cells. (e) Frequencies of CTV^{low} OT-
619 I cells. Data are mean ± SEM of technical triplicates. Statistical significance was
620 determined by one-way ANOVA followed by Dunnett's multiple-comparison test.
621

622 **Fig 2. In vivo generation of designer APCs stimulates antigen-specific $CD8^+$**
623 **T cells**

624 (a) C57BL/6 mice received three weekly i.v. injections (days 0, 7, 14) of control
625 mRNA, OVA-MITD mRNA (5 μg + 10 μg control), or OVA-MITD + CD80 +
626 membrane-anchored IL-2 mRNAs (5 μg each; total 15 μg). Spleens were
627 collected 7 d after the final dose. (b) Representative dot plots of OVA-specific
628 $CD8^+$ T cells. (c) Number of $tetramer^+$ $CD8^+$ T cells in the spleens. (d) Number of
629 IFN-γ^+ $CD8^+$ T cells. (e) Mice were subcutaneously inoculated with OVA-
630 expressing EL-4 cells (E.G7), followed by intravenous administration of mRNAs
631 on days 7, 14, and 21. (f) Tumor growth curves are presented. (g) Kaplan-Meier
632 survival curve. (h) E.G7 cells were subcutaneously implanted into C57BL/6 mice.
633 When tumors reached ~100 mm^3, mice received intravenous injections of control

634 mRNA, OVA-MITD mRNA alone, or a combination of mRNAs. Tumor-infiltrating
635 lymphocytes were analyzed one week later. (i) Representative dot plots of TILs.
636 (j) Number of tetramer$^+$ CD8$^+$ T cells. (k) Number of IFN-γ$^+$ CD8$^+$ T cells. Data
637 are mean ± SEM. Statistical significance was assessed by using an unpaired,
638 two-tailed Student's t-test (c, d, j, k) and by the log-rank (Mantel-Cox) test for
639 survival analysis (g).
640
641 **Fig 3. In vivo generation of designer APCs expands neoantigen-specific**
642 **CD8$^+$ T cells**
643 (a) C57BL/6 mice received three weekly i.v. injections (days 0, 7, 14) of control
644 mRNA (15 μg), Rpl18-MITD mRNA (5 μg) + control mRNA (10 μg), or Rpl18-
645 MITD (5 μg)+ CD80(5 μg) + membrane-anchored IL-2(5 μg) mRNAs. Spleens
646 were collected 7 d after the final dose. (b) Representative dot plots of Rpl18-
647 specific CD8$^+$ T cells in the spleens. (c) Number of tetramer$^+$ CD8$^+$ T cells in the
648 spleens. (d) Number of IFN-γ$^+$ CD8$^+$ T cells in the spleens. (e) Mice were
649 subcutaneously inoculated Rpl18-MC38 cells, followed by intravenous
650 administration of mRNAs on days 7, 14, and 21. (f) Tumor growth curves are
651 presented. (g) Kaplan-Meier survival curves of tumor-bearing mice. Data are
652 mean ± SEM. Statistical significance for (c,d) was determined by using an
653 unpaired, two-tailed Student's t-test, and survival differences in (g) by the log-
654 rank (Mantel-Cox) test.
655
656 **Fig 4. Generation of humanized designer APCs activates NY-ESO-1-specific**
657 **CD8$^+$ T cells**

658 (a) HLA-A*02:01 transgenic mice received a single i.v. dose of control mRNA (15
659 μg), NY-ESO-1-MITD mRNA (5 μg) plus control mRNA (10 μg), or NY-ESO-1-
660 MITD (5 μg) + mouse CD80 (5 μg) + membrane-anchored mouse IL-2 (5 μg)
661 mRNAs. The spleens were collected 7 d later. (b) Representative dot plots of NY-
662 ESO-1-specific $CD8^+$ T cells in the spleens. (c) Number of $tetramer^+$ $CD8^+$ T cells
663 in the spleens. (d) Number of IFN-γ^+ $CD8^+$ T cells in the spleen. (e) In vivo killing
664 assay: on day 0 mice were treated as in (a). On day 7, 1×10^6 NY-ESO-1-pulsed
665 splenocytes (CTV-labelled) and 1×10^6 control-peptide-pulsed splenocytes
666 (CFSE-labelled) were transferred i.v.; 24 h later, spleens were harvested and
667 target-cell killing was analysed by flow cytometry. (f) Representative dot plots of
668 CTV^+ and $CFSE^+$ target cells. (g) Ratio of $CTV^+/CFSE^+$ cells in spleen. (h)
669 Schematic of the in vitro co-culture assay. (i) Representative dot plots of NY-ESO-
670 1-TCR (Venus) positive CD8 T cells. (j) IFN-γ expression in NYESO1-TCR^+ and
671 polyclonal T cells after 3 days of stimulation with HEK293 cells transfected with
672 control mRNA, NYESO1-MITD mRNA, or a mixture of NYESO1-MITD, hCD80,
673 and hIL-2 mRNAs. Statistical significance was determined using an unpaired,
674 two-tailed Student's t-test for panels (c), (d), and (g), and using two-way ANOVA
675 followed by Tukey's multiple comparisons test for panel (j).
676

677 **Fig 5. In vivo generation of designer APCs induces Th1 differentiation of**
678 **antigen-specific $CD4^+$ T cells**

679 (a) Schematic representation of the mRNA construct encoding OVA-MHC-II,
680 CD80 and membrane-anchored IL-12. (b) C57BL/6 mice received two weekly i.v.
681 injections of control mRNA (15 μg), OVA-MHC-II mRNA (5 μg) plus control mRNA

682 (10 μg), or OVA-MHC-II (5 μg) + CD80 (5 μg) + membrane-anchored-IL-12 (5 μg)
683 mRNAs. The spleens were collected 7 d after the final dose. (c) Representative
684 dot plots of OVA-specific $CD4^+$ T cells in the spleens. (d) Number of $tetramer^+$
685 $CD4^+$ T cells in the spleens. (e) Representative dot plots of T-bet^+ OVA-specific
686 $CD4^+$ T cells in the spleens. (f) Number of T-bet^+ OVA-specific $CD4^+$ T cells in the
687 spleens. (g) Number of IFN-γ^+ $CD4^+$ T cells in the spleens. Data are mean ± SEM.
688 Statistical significance for panels (d,f,g) was determined by using an unpaired,
689 two-tailed Student's t-test.

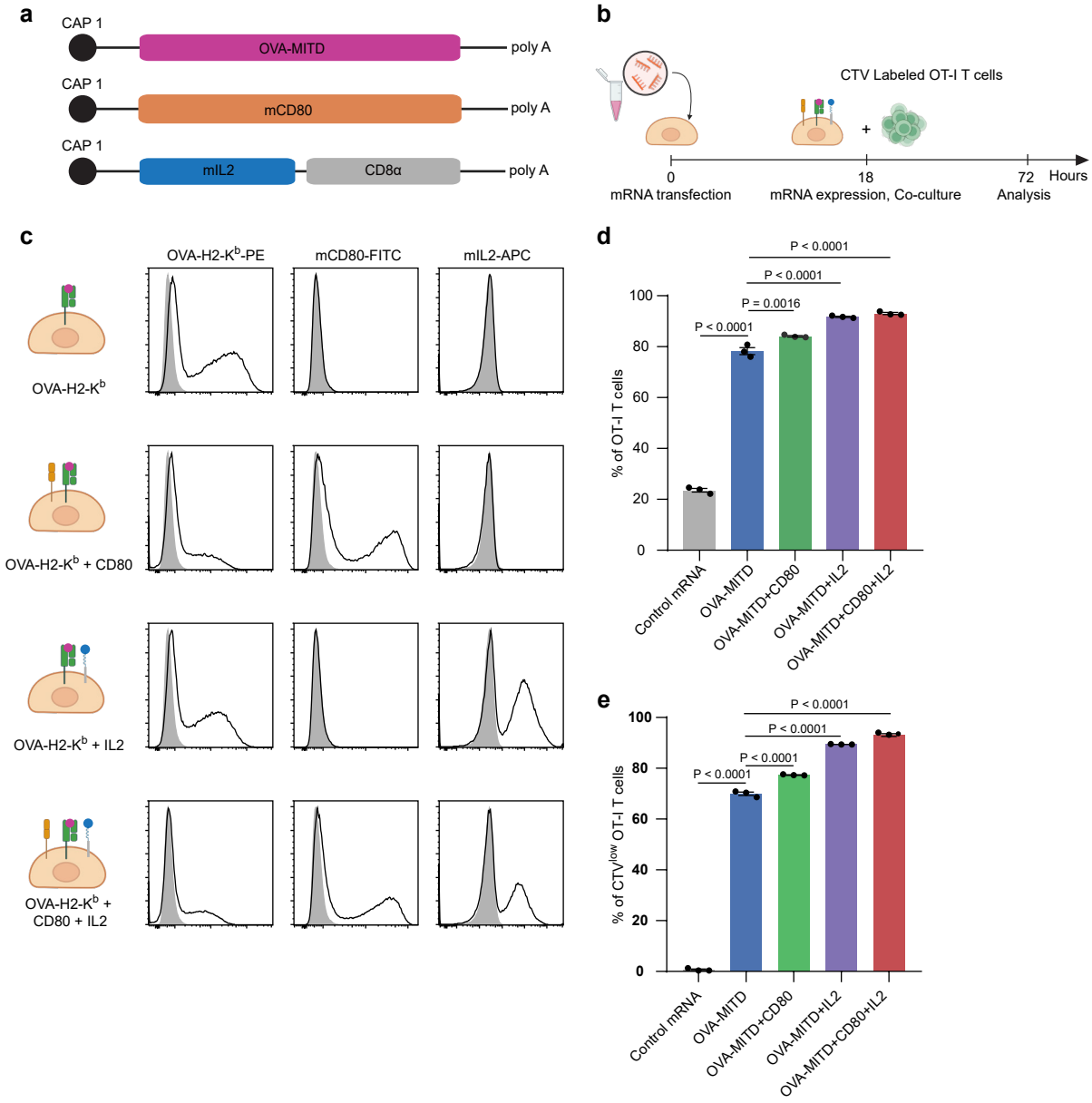
a
CAP 1
OVA-MITD
poly A
CAP 1
mCD80
poly A
CAP 1
mIL2
CD8α
poly A
b
CTV Labeled OT-I T cells
0
18
72
Hours
mRNA transfection
mRNA expression, Co-culture
Analysis
c
OVA-H2-Kb-PE
mCD80-FITC
mIL2-APC
OVA-H2-Kb
OVA-H2-Kb + CD80
OVA-H2-Kb + IL2
OVA-H2-Kb + CD80 + IL2
d
% of OT-I T cells
P < 0.0001
P < 0.0001
P = 0.0016
P < 0.0001
Control mRNA
OVA-MITD
OVA-MITD+CD80
OVA-MITD+IL2
OVA-MITD+CD80+IL2
e
% of CTVlow OT-I T cells
P < 0.0001
P < 0.0001
P < 0.0001
P < 0.0001
Control mRNA
OVA-MITD
OVA-MITD+CD80
OVA-MITD+IL2
OVA-MITD+CD80+IL2

Fig 1. Le, et al.

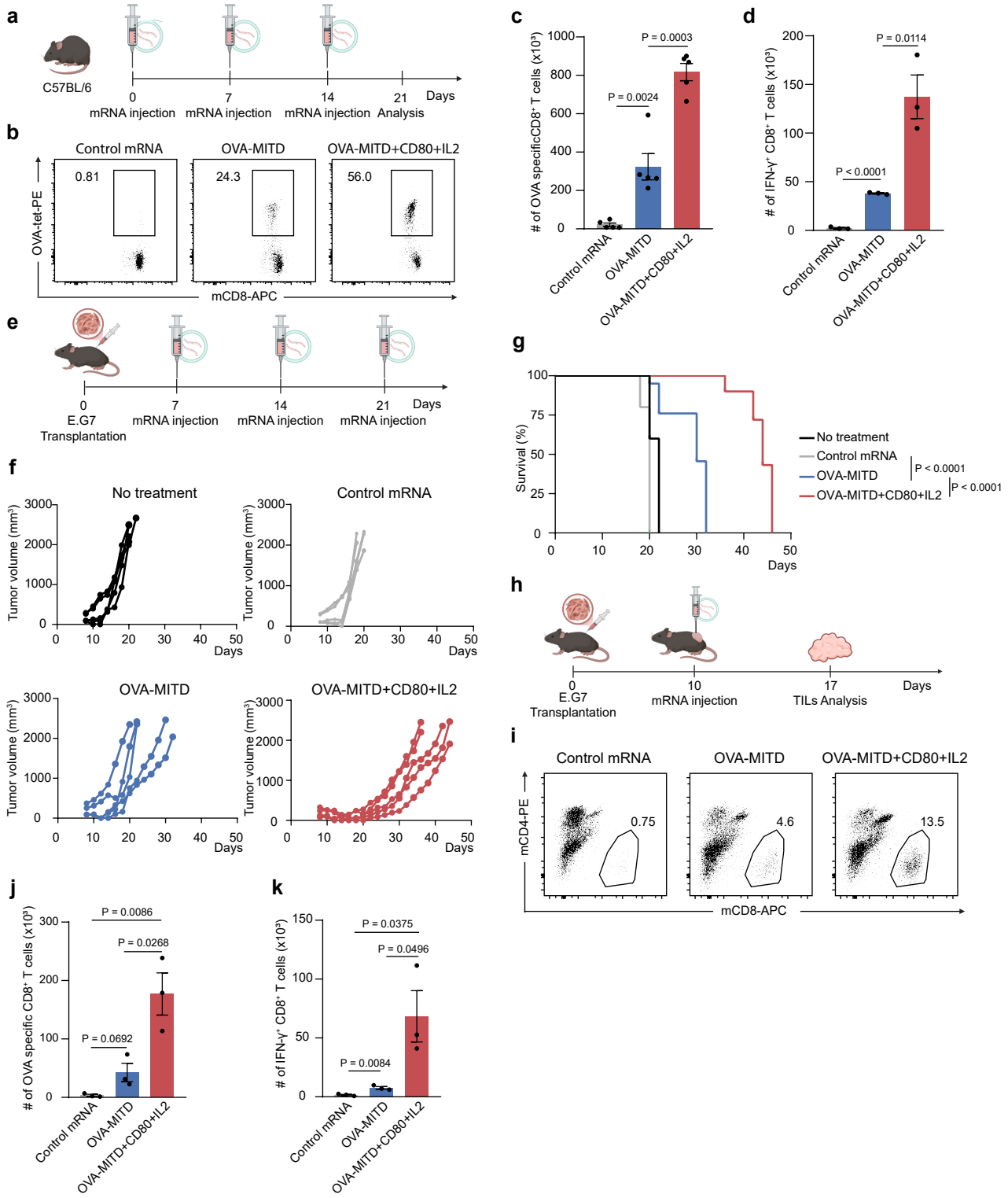
a
C57BL/6
0
mRNA injection
7
mRNA injection
14
mRNA injection
21
Analysis
Days
b
Control mRNA
OVA-MITD
OVA-MITD+CD80+IL2
0.81
24.3
56.0
OVA-tet-PE
mCD8-APC
c
P = 0.0003
P = 0.0024
# of OVA specificCD8+ T cells (x10³)
Control mRNA
OVA-MITD
OVA-MITD+CD80+IL2
d
P = 0.0114
P < 0.0001
# of IFN-γ+ CD8+ T cells (x10³)
e
0
E.G7
Transplantation
7
mRNA injection
14
mRNA injection
21
mRNA injection
Days
f
No treatment
Control mRNA
OVA-MITD
OVA-MITD+CD80+IL2
Tumor volume (mm³)
Days
g
Survival (%)
Days
No treatment
Control mRNA
OVA-MITD
OVA-MITD+CD80+IL2
P < 0.0001
P < 0.0001
h
0
E.G7
Transplantation
10
mRNA injection
17
TILs Analysis
Days
i
Control mRNA
OVA-MITD
OVA-MITD+CD80+IL2
0.75
4.6
13.5
mCD4-PE
mCD8-APC
j
P = 0.0086
P = 0.0268
P = 0.0692
# of OVA specific CD8+ T cells (x10³)
k
P = 0.0375
P = 0.0496
P = 0.0084
# of IFN-γ+ CD8+ T cells (x10³)

Fig 2. Le, et al.

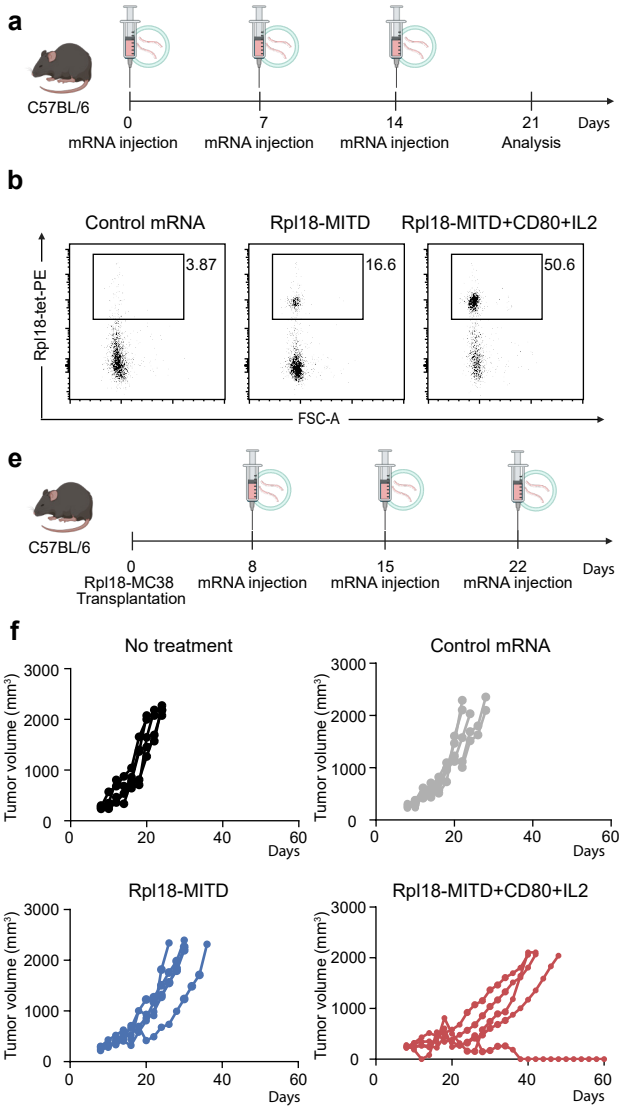
a
C57BL/6
0
mRNA injection
7
mRNA injection
14
mRNA injection
21
Analysis
Days
b
Control mRNA
Rpl18-MITD
Rpl18-MITD+CD80+IL2
Rpl18-tet-PE
3.87
16.6
50.6
FSC-A
e
C57BL/6
0
Rpl18-MC38
Transplantation
8
mRNA injection
15
mRNA injection
22
mRNA injection
Days
f
No treatment
Control mRNA
Rpl18-MITD
Rpl18-MITD+CD80+IL2
Tumor volume (mm³)
Days

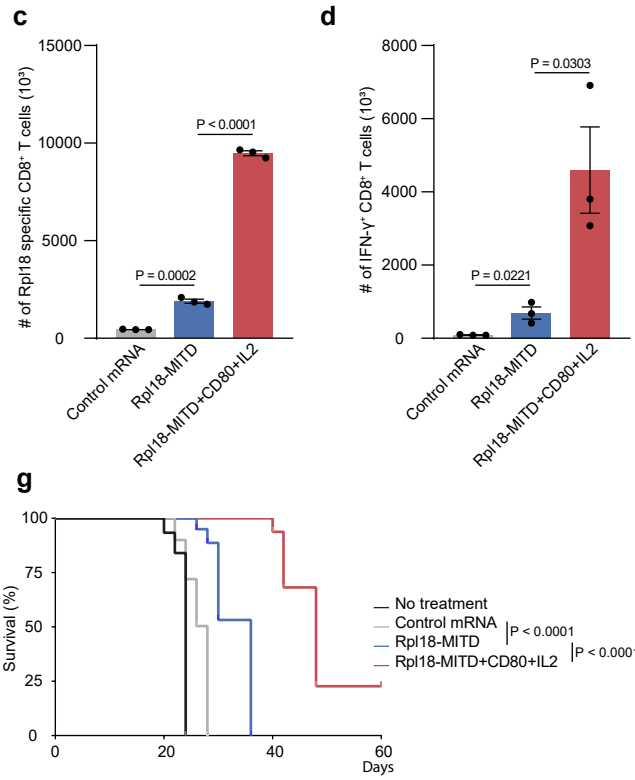
c
# of Rpl18 specific CD8⁺ T cells (10³)
P = 0.0002
P < 0.0001
Control mRNA
Rpl18-MITD
Rpl18-MITD+CD80+IL2
d
# of IFN-γ⁺ CD8⁺ T cells (10³)
P = 0.0221
P = 0.0303
g
Survival (%)
Days
No treatment
Control mRNA
Rpl18-MITD
Rpl18-MITD+CD80+IL2
P < 0.0001
P < 0.0001

Fig 3. Le, et al.

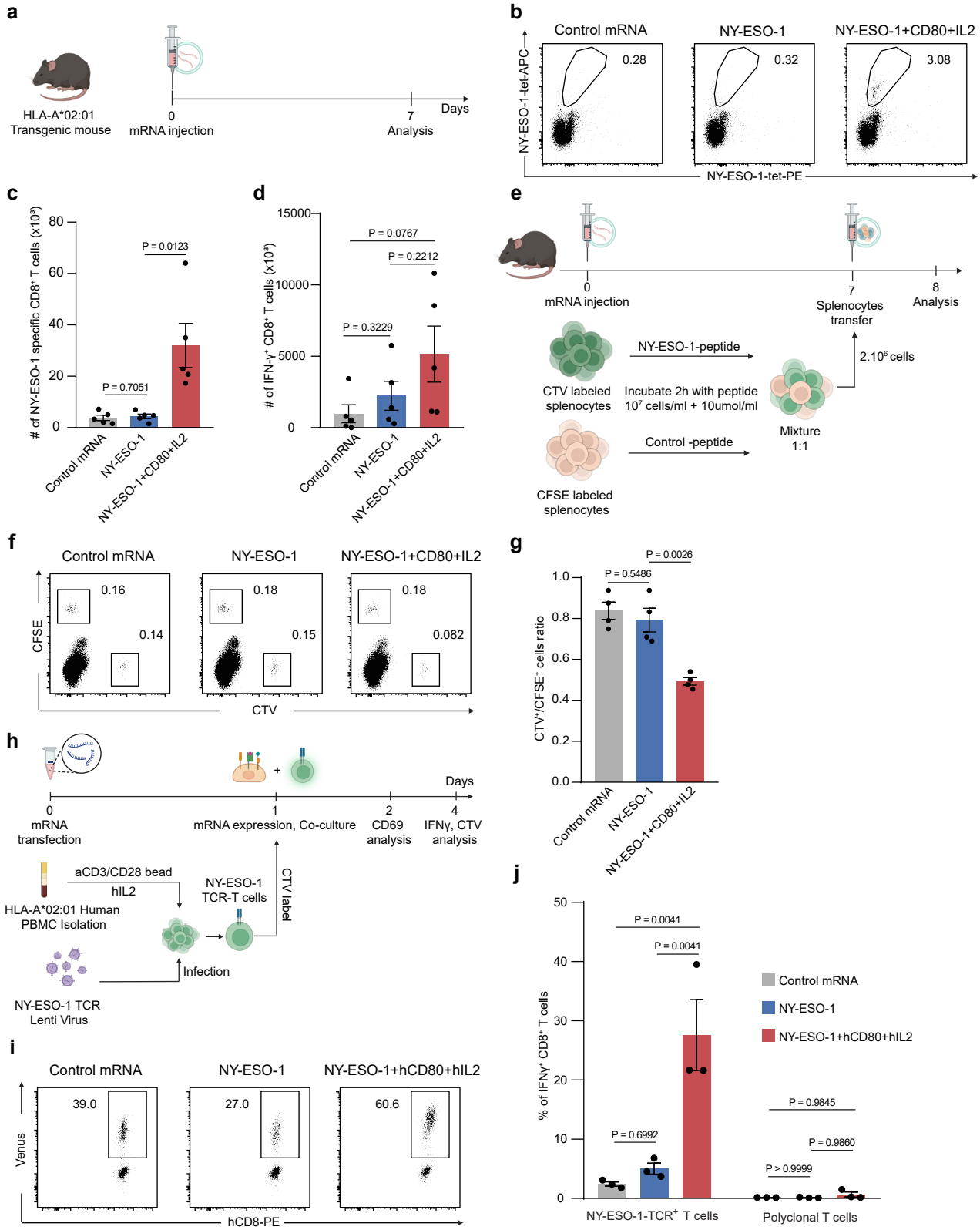
a
HLA-A*02:01
Transgenic mouse
0
mRNA injection
7
Analysis
Days
b
Control mRNA
NY-ESO-1
NY-ESO-1+CD80+IL2
0.28
0.32
3.08
NY-ESO-1-tet-APC
NY-ESO-1-tet-PE
c
# of NY-ESO-1 specific CD8+ T cells (x10³)
P = 0.0123
P = 0.7051
Control mRNA
NY-ESO-1
NY-ESO-1+CD80+IL2
d
# of IFN-γ+ CD8+ T cells (x10³)
P = 0.0767
P = 0.2212
P = 0.3229
Control mRNA
NY-ESO-1
NY-ESO-1+CD80+IL2
e
0
mRNA injection
7
Splenocytes transfer
8
Analysis
CTV labeled splenocytes
NY-ESO-1-peptide
Incubate 2h with peptide
10⁷ cells/ml + 10umol/ml
2.10⁶ cells
Mixture 1:1
CFSE labeled splenocytes
Control -peptide
f
Control mRNA
NY-ESO-1
NY-ESO-1+CD80+IL2
0.16
0.14
0.18
0.15
0.18
0.082
CFSE
CTV
g
P = 0.0026
P = 0.5486
CTV+/CFSE+ cells ratio
Control mRNA
NY-ESO-1
NY-ESO-1+CD80+IL2
h
Days
0
mRNA transfection
1
mRNA expression, Co-culture
2
CD69 analysis
4
IFNγ, CTV analysis
aCD3/CD28 bead
hIL2
HLA-A*02:01 Human PBMC Isolation
NY-ESO-1 TCR-T cells
CTV label
Infection
NY-ESO-1 TCR Lenti Virus
i
Control mRNA
NY-ESO-1
NY-ESO-1+hCD80+hIL2
39.0
27.0
60.6
Venus
hCD8-PE
j
P = 0.0041
P = 0.0041
P = 0.6992
P = 0.9845
P = 0.9860
P > 0.9999
% of IFNγ+ CD8+ T cells
Control mRNA
NY-ESO-1
NY-ESO-1+hCD80+hIL2
NY-ESO-1-TCR+ T cells
Polyclonal T cells

Fig 4. Le, et al.

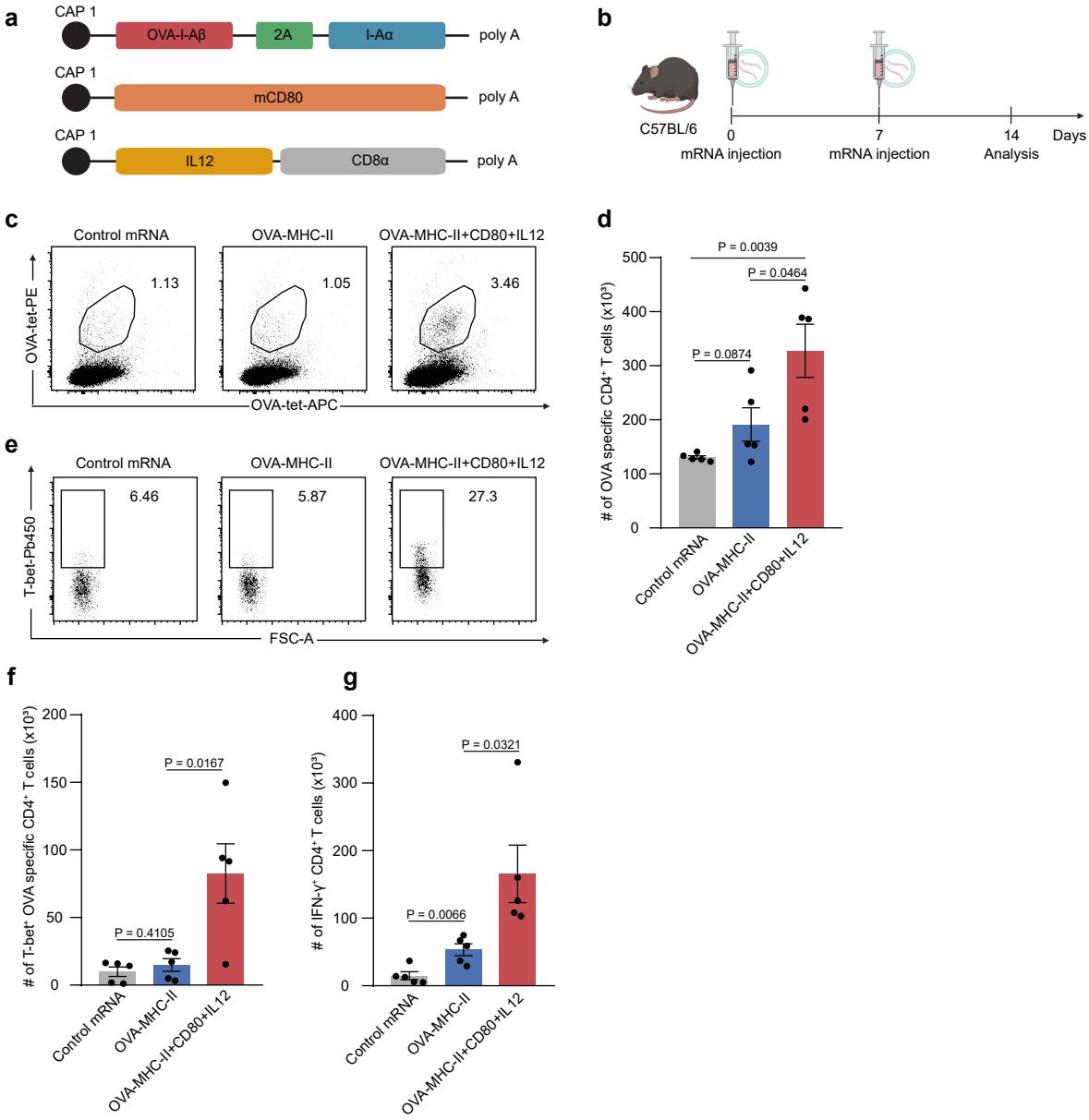
a
CAP 1
OVA-I-Aβ
2A
I-Aα
poly A
CAP 1
mCD80
poly A
CAP 1
IL12
CD8α
poly A
b
C57BL/6
0
mRNA injection
7
mRNA injection
14
Analysis
Days
c
Control mRNA
OVA-MHC-II
OVA-MHC-II+CD80+IL12
1.13
1.05
3.46
OVA-tet-PE
OVA-tet-APC
d
P = 0.0039
P = 0.0464
P = 0.0874
# of OVA specific CD4+ T cells (x10³)
500
400
300
200
100
0
Control mRNA
OVA-MHC-II
OVA-MHC-II+CD80+IL12
e
Control mRNA
OVA-MHC-II
OVA-MHC-II+CD80+IL12
6.46
5.87
27.3
T-bet-Pb450
FSC-A
f
# of T-bet+ OVA specific CD4+ T cells (x10³)
200
150
100
50
0
P = 0.0167
P = 0.4105
Control mRNA
OVA-MHC-II
OVA-MHC-II+CD80+IL12
g
# of IFN-γ+ CD4+ T cells (x10³)
400
300
200
100
0
P = 0.0321
P = 0.0066
Control mRNA
OVA-MHC-II
OVA-MHC-II+CD80+IL12

Fig 5. Le, et al.

a

OVA-MITD amino acids sequence

Signal sequence | Linker | OVA-peptide

MRVTAPRTLILLLSGALALTETWAGSGGSGGGGSGGSVSGLEQLESIINFEKLTEWTSSNVMEERKIKVYLPRMKMEEKYNLTSVLMAMGITDVFSSSANLSGISSAESLKISQAV

Linker | MHC class I trafficking domain sequence

HAAHAEINEAGREVVGSAEAGGSLGGGGSGIVGIVAGLAVLAVVVIGAVVATVMCRRKSSGGKGGSYSQAASSDSAQGSDVSLTA

b

Mouse CD80 amino acids sequence

Signal sequence | mouse CD80

MACNCQLMQDTPLLKFPCPRLILLFVLLIRLSQVSSDVDEQLSKSVKDKVLLPCRYNSPHEDESEDRIYWQKHDKVVLSVIAGKLKVWPEYKNRTLYDNTTYSLIILGLVLSDRGTY

SCVVQKKERGTYEVKHLALVKLSIKADFSTPNITESGNPSADTKRITCFASGGFPKPRFSWLENGRELPGINTTISQDPESELYTISSQLDFNTTRNHTIKCLIKYGDAHVSEDFTWE

KPPEDPPDSKNTLVLFGAGFGAVITVVVIVVIIKCFCKHRSCFRRNEASRETNNSLTFGPEEALAEQTVFL

c

Mouse IL2-CD8 amino acids sequence

Signal sequence | mouse IL2

MYSMQLASCVTLTLVLLVNSAPTSSSTSSSTAEAQQQQQQQQQQQQHLEQLLMDLQELLSRMENYRNLKLPRMLTFKFYLPKQATELKDLQCLEDELGPLRHVLDLTQSKSFQ

Linker | mouse CD8α

LEDAENFISNIRVTVVKLKGSDNTFECQFDDESATVVDFLRRWIAFCQSIISTSPQGGGGSVISNSVMYFSSVVPVLQKVNSTTTKPVLRTPSPVHPTGTSQPQRPEDCRPRGSV

KGTGLDFACDIYIWAPLAGICVALLLSLIITLICYHRSRKRVCKCPRPLVRQEGKPRPSEKIV

d

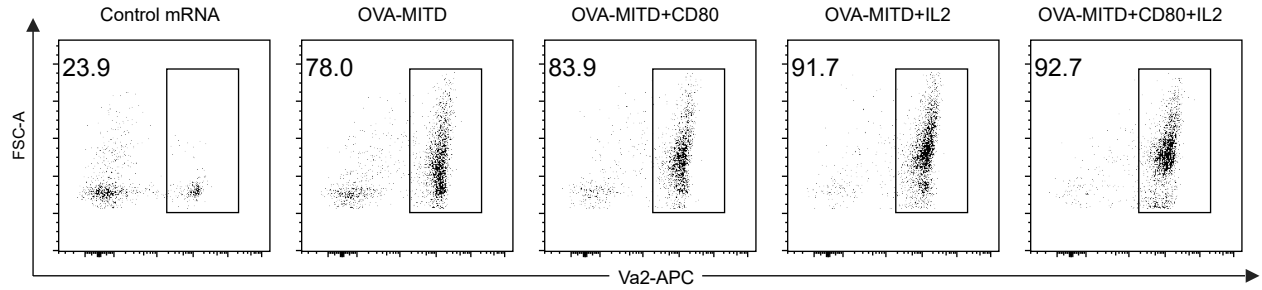

e

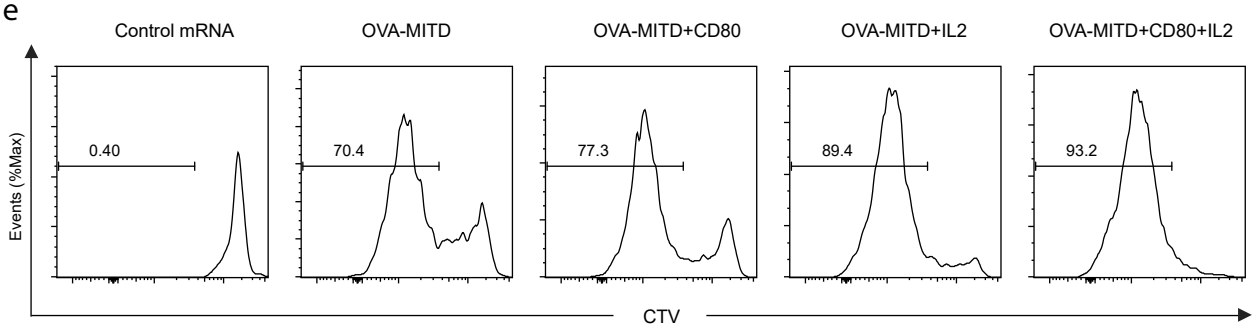

Supplementary Figure 1. Le, et al.

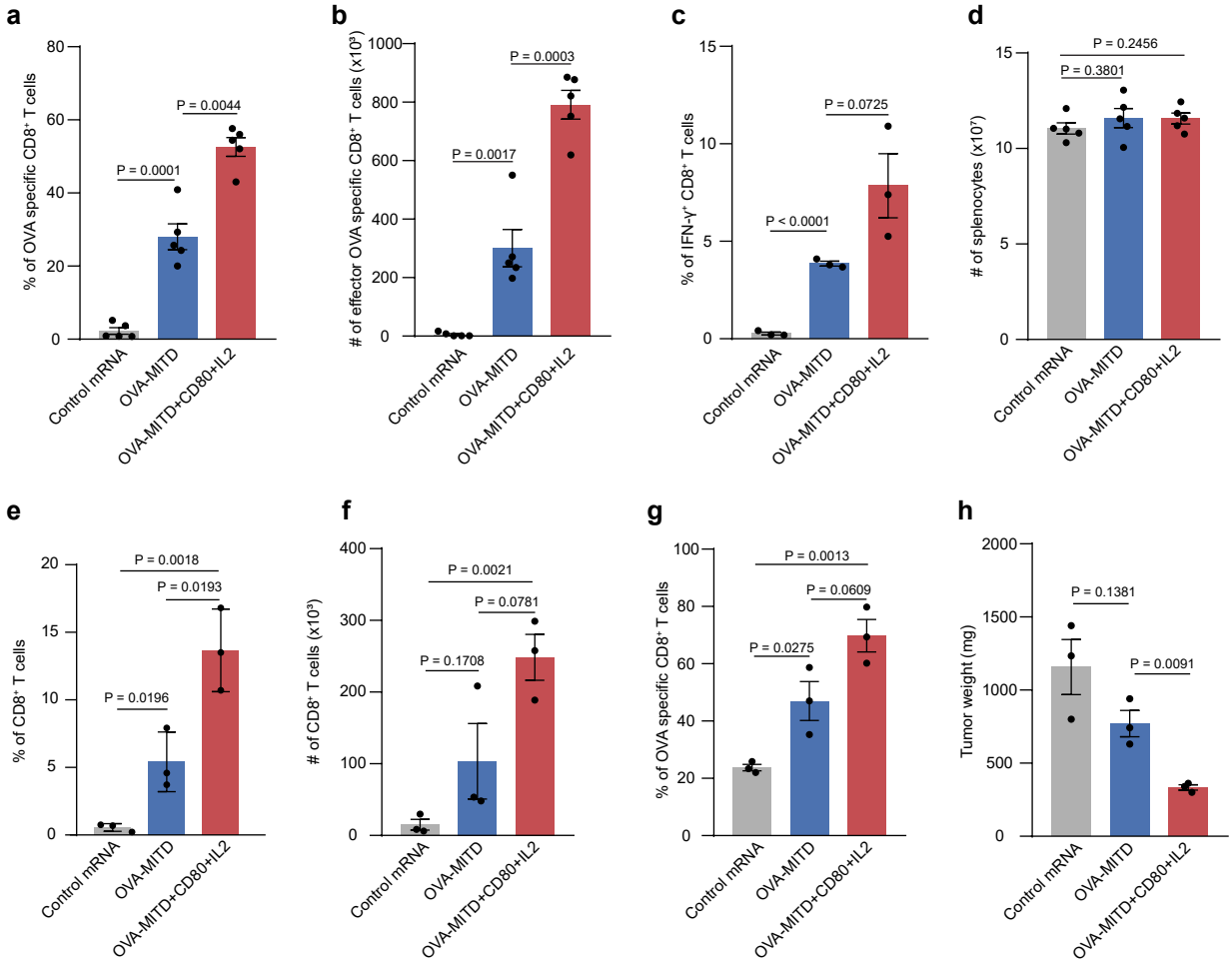

Supplementary Figure 2. Le, et al.

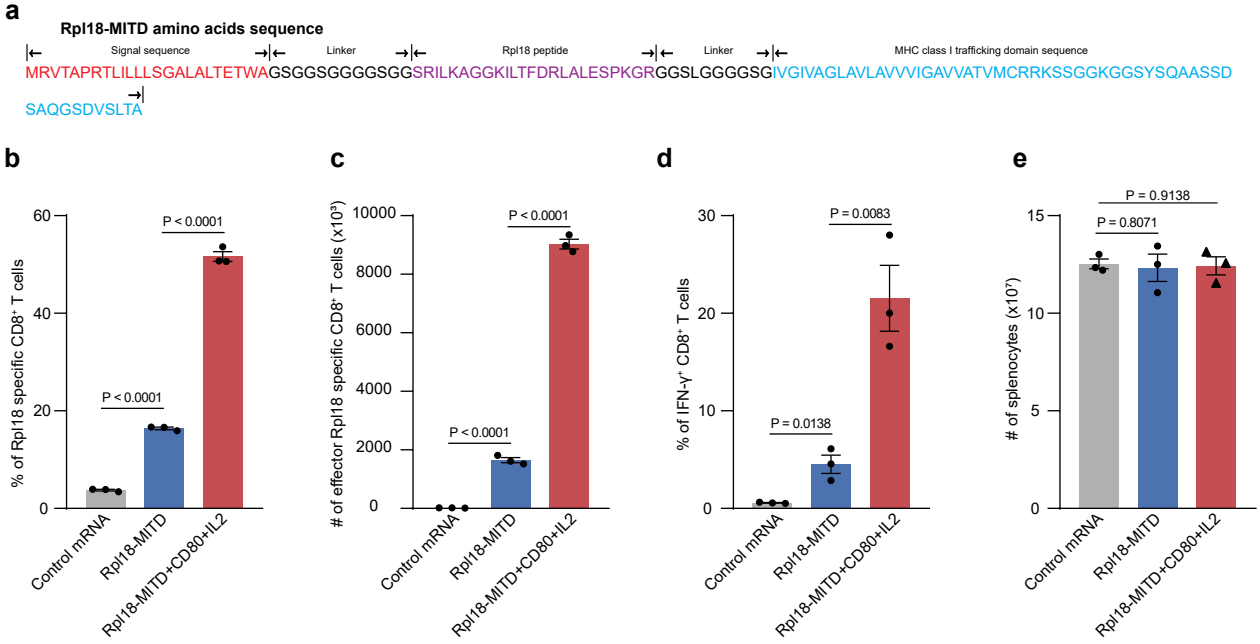

Supplementary Figure 3. L, et al.

a NY-ESO-1-MITD amino acids sequence

Signal sequence | Linker | NY-ESO-1 peptide | Linker | MHC class I trafficking domain sequence

MRVTAPRTLILLLSGALALTETWAGSGGSGGGGSGGISSCLQQLSLLMWITQCFLPVFLAQGGSLGGGGSGIVGIVAGLAVLAVVVIGAVVATVMCRRKSSGGKGGSYSQAASS

DSAQGSDVSLTA

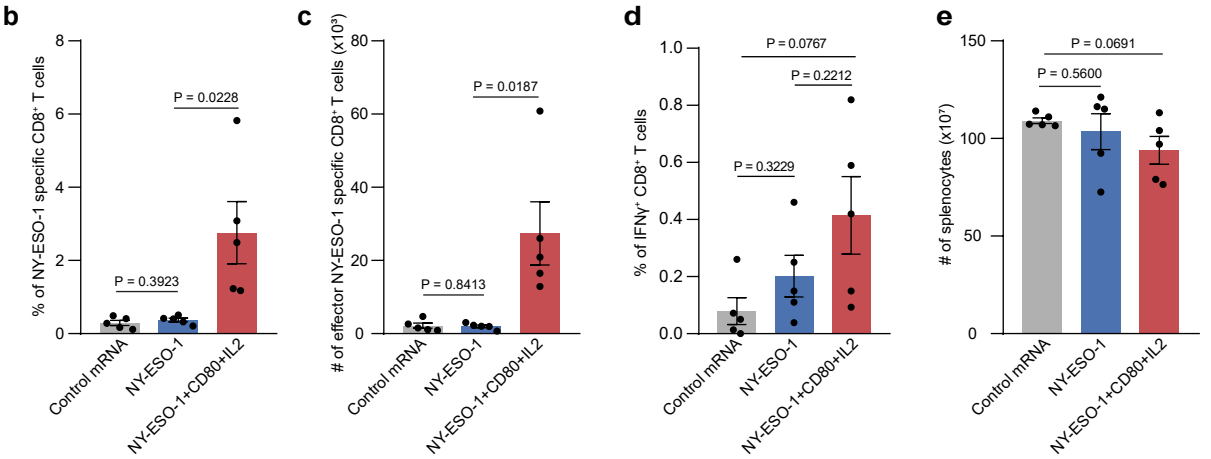

f Human CD80 amino acid sequence

Signal sequence | human CD80

MGHTRRQGTSPSKCPYLNFFQLLVLAGLSHFCSGVIHVTKEVKEVATLSCGHNVSVEELAQTRIYWQKEKKMVLTMMSGDMNIWPEYKNRTIFDITNNLSIVILALRPSDEGTYE

CVVLKYEKDAFKREHLAEVTLSVKADFPTPSISDFEIPTSNIRRIICSTSGGFPEPHLSWLENGEELNAINTTVSQDPETELYAVSSKLDFNMTTNHSFMCLIKYGHLRVNQTFNW

NTTKQEHFPDNLLPSWAITLISVNGIFVICCLTYCFAPRCRERRRNERLRRESVRPV

g Human IL2-CD8 amino acid sequence

Signal sequence | IL2 | Linker | human CD8

MYRMQLLSCIALSLALVTNSAPTSSSTKKTQLQLEHLLLDLQMILNGINNYKNPKLTRMLTFKFYMPKKATELKHLQCLEEELKPLEEVLNLAQSKNFHLRPRDLISNINVIVLELKGS

ETTFMCEYADETATIVEFLNRWITFCQSIISTLTGGGGSFVPVFLPAKPTTTPAPRPPTTQRFSGPAPTIASQPLSLRPEACRPAAGGAVHTRGLDFACDIYIWAPLAGTCGVLLLSLV

ITLYCNHRNRRRVCKCPRPVVKSGDKPSLSARYV

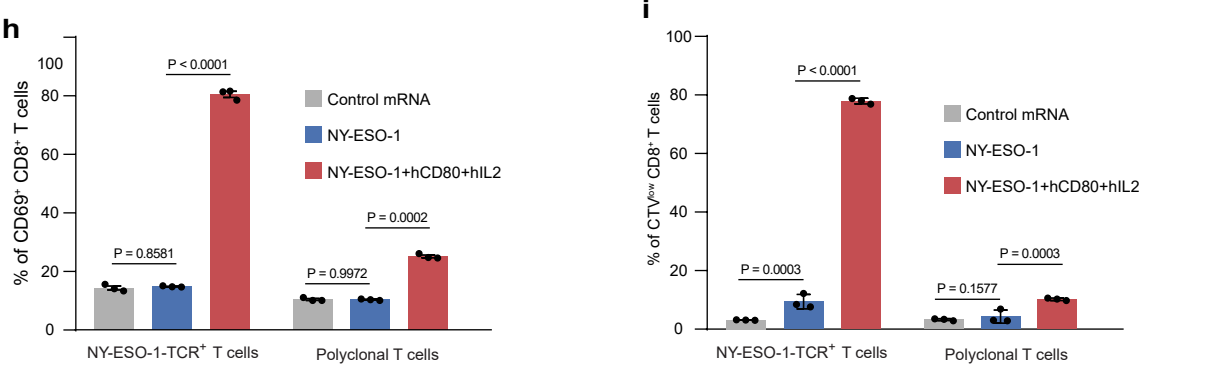

Supplementary Figure 4. Le, et al.

a **Mouse OVA-MHC-II aminoacids sequence**

Signal sequence | OVA peptide | Linker | I-Aβ

MALQIPSLLLSAAVVVLMVLSSPGTEGISQAVHAAHAEINEAGRGGGGSGGGGSGGDSERHFVYQFMGECYFTNGTQRIRYVTRYIYNREEYVRYDSDVGEHRAVTELGRPDA

EYWNSQPEILERTRAELDTVCRHNYEGPETHTSLRRLEQPNVVISLSRTEALNHHNTLVCSVTDFYPAKIKVRWFRNGQEETVGVSSTQLIRNGDWTFQVLVMLEMTPRRGEVY

2A

TCHVEHPSLKSPITVEWRAQSESAWSKMLSGIGGCVLGVIFLGLGLFIRHRSQKGPRGPPPAGLLQGSGATNFSLLKQAGDVEENPGPMPRSRALILGVLALTTMLSLCGGEDD

I-Aα

IEADHVGTYGISVYQSPGDIGQYTFEFDGDELFYVDLDKKETVWMLPEFGQLASFDPQGGLQNIAVVKHNLGVLTKRSNSTPATNEAPQATVFPKSPVLLGQPNTLICFVDNIFPP

VINITWLRNSKSVADGVYETSFFVNRDYSFHKLSYLTFIPSDDDIYDCKVEHWGLEEPVLKHWEPEIPAPMSELTETVVCALGLSVGLVGIVVGTIFIIQGLRSGGTSRHPGPL

b

Mouse IL12-CD8 amino acids sequence

Signal sequence | mouse IL12B

MCPQKLTISWFAIVLLVSPLMAMWELEKDVYVVEVDWTPDAPGETVNLTCDTPEEDDITWTSDQRHGVIGSGKTLTITVKEFLDAGQYTCHKGGETLSHS HLLLHKKENGIWST

EILKNFKNKTFLKCEAPNYSGRFTCSWLVQRNMDLKFNIKSSSSSPDSRAVTCGMASLSAEKVTLDQRDYEKYSVSCQEDVTCPTAEETLPIELALEARQQNKYENYSTSFFIRD

IIKPDPPKNLQMKPLKNSQVEVSWEYPDSWSTPHSYFSLKFFVRIQRKKEKMKETEEGCNQKGAFLVEKTSTEVQCKGGNVCVQAQDRYYNSSCSKWACVPCRVRSGGGGS

Linker | mouse IL12A

GGGGSGGGGSRVIPVSGPARCLSQSRNLLKTTDDMVKTAREKLKHYSCTAEDIDHEDITRDQTSTLKTCLPLELHKNESCLATRETSSTTRGSCLPPQKTSLMMTLCLGSIYEDL

Linker

KMYQTEFQAINAALQNHNHQQIILDKGMLVAIDELMQSLNHNGETLRQKPPVGEADPYRVKMKLCILLHAFSTRVVTINRVMGYLSSAGGGGSDYKDDDDKVISNSVMYFSSVV

mouse CD8

PVLQKVNSTTTKPVLRTPSPVHPTGTSQPQRPEDCRPRGSVKGTGLDFACDIYIWAPLAGICVALLLSLIITLICYHRSRKRVCKCPRPLVRQEGKPRPSEKIV

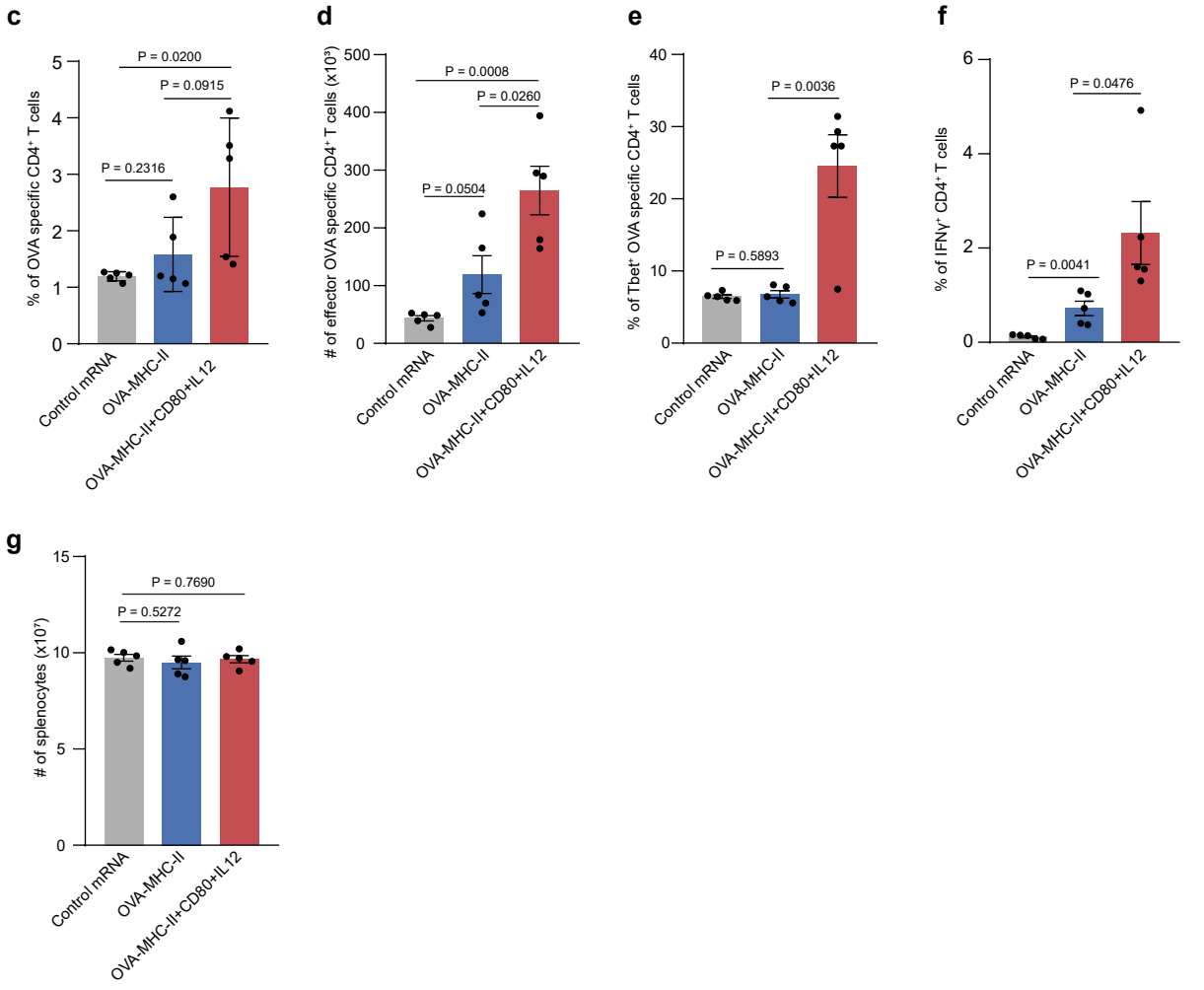

Supplementary Figure 5. Le, et al.

Supplementary Figure 1. Designer APC-mediated stimulation of $CD8^+$ T cells

(a-c) Amino acid sequences of OVA-MITD, mouse CD80, and membrane-anchored mouse IL-2 used for mRNA synthesis. (d, e) Representative flow cytometry plots showing OT-I $CD8^+$ T cells and proliferating (CTV^{low}) OT-I cells after co-culture with designer APCs.

Supplementary Figure 2. Designer APC-induced activation of antigen-specific $CD8^+$ T Cells in spleen and tumor

(a) Frequencies of OVA-specific $CD8^+$ T cells in the spleens. (b) Number of $CD44^{hi}CD62L^{low}$ $CD8^+$ T cells in the spleens. (c) Frequencies of IFN-γ^+ $CD8^+$ T cells in the spleens. (d) Number of total splenocytes. (e) Frequencies of $CD8^+$ T cells in the tumors. (f) Quantification of $CD8^+$ T cells per 100 mg tumors. (g) Frequencies of OVA-specific $CD8^+$ T cells in TILs. (h) Tumor weight at harvest. Data are presented as mean ± SEM. Statistical significance was assessed using unpaired, two-tailed Student's *t*-test.

Supplementary Figure 3. Activation of neoantigen-specific $CD8^+$ T cells by designer APCs

(a) Amino acid sequence of Rpl18-MITD. (b) Frequencies of Rpl18-specific $CD8^+$ T cells in the spleens. (c) Number of $CD4^{hi}CD62L^{low}$ $CD8^+$ T cell in the spleens. (d) Frequencies of IFN-γ^+ $CD8^+$ T cells in the spleens. (e) Number of total splenocytes. Data are presented as mean ± SEM. Statistical significance was assessed using unpaired, two-tailed Student's *t*-test.

25

26 **Supplementary Figure 4. Humanized designer APCs activate antigen-**
27 **specific CD8$^+$ T cells**

28 (a) Amino acid sequence of NY-ESO-1-MITD. (b) Frequencies of NY-ESO-1
29 specific CD8$^+$ T cells. (c) Number of CD44^{hi}CD62L^{low} NY-ESO-1 specific CD8$^+$ T
30 cell in the spleens. (d) Frequencies of IFN-γ$^+$ CD8$^+$ T cells in the spleens. (e)
31 Number of total splenocytes. (f) Amino acid sequence of human CD80. (g) Amino
32 acid sequence of membrane-anchored human IL-2. (h) Frequencies of CD69$^+$
33 CD8 T cells. (i) Frequencies of CTV^{low} CD8$^+$ T cells. Data are presented as mean
34 ± SEM. Statistical significance was determined using an unpaired, two-tailed
35 Student's t-test for panels (b-e), and two-way ANOVA followed by Tukey's multiple
36 comparisons test for panels (h) and (i).

37

38 **Supplementary Figure 5. Induction of Th1 cells by designer APCs**

39 (a) Amino acid sequence of membrane-anchored mouse IL-12. (b) Schematic of
40 OVA peptide fused to MHC-II. (c) Frequencies of OVA-specific CD4$^+$ T cells. (d)
41 Number of CD44^{hi}CD62L^{low} CD4$^+$ T cell phenotype. (e) Frequencies of T-bet$^+$
42 CD4$^+$ T cells. (f) Frequencies of IFN-γ$^+$ OVA-specific CD4$^+$ T cells. (g) Number of
43 total splenocytes. Data are presented as mean ± SEM. Statistical significance
44 was assessed using unpaired, two-tailed Student's *t*-test.

45

46